A dynamic modelling approach to evaluating volume vs mass-based variable buoyancy underwater gliders

Henry Dawson
220170682

A dissertation submitted in fulfilment of the partial requirements
for the Bachelor of Engineering in
Marine Technology with Small Craft Tech
School of Engineering
Newcastle University
May 2026

Supervisor: Dr. Andrew Aspden

Declaration

No part of the work presented in this thesis has been submitted in support of another degree or qualification of this or any other university or other institute of learning.

Abstract

Energy consumption and manoeuvring performance are two key components of an underwater glider's effectiveness in oceanographic research missions. This study aims to compare mass-variable and volume-variable buoyancy propulsors, with respect to underwater glider energy consumption and manoeuvrability. By formulating a dynamic model using the Newton-Euler equations of motion, this study assessed the energy consumption and motion of the two UG systems in idealised fluid conditions. Using this, it was shown that there is a marginal benefit to using a mass-variable UG over a volume-variable UG in sawtooth motion, and when station-keeping with a spiral descent. The mass-variable UG presented an 82.2 to 200.6% reduction in attitude adjustment work across pitch angles of 20 to 40° in a sawtooth profile and a lowered bank overshoot in the spiral test due to the more stable roll response. This study contributes to the improvement of underwater glider design rationale, and identifies future work to formalise the findings stated.

Keywords

Underwater glider, Dynamic Modelling, Variable Buoyancy, Volume Variable Buoyancy System, Mass Variable Buoyancy System

1 Introduction

1.1 Motivation

Buoyancy propelled underwater gliders (UGs) have seen a wide adoption in Oceanographic research fields since their initial conception by Stommel (1989), due to their low energy cost in comparison to conventionally propelled autonomous underwater vehicles (AUVs) (Carneiro et al., 2024; Phillips et al., 2012). Energy consumption optimisation remains an important research focus when developing UGs, as it benefits not only mission endurance and longevity, but the quality of collected data. Rudnick et al. (2004) explained how powering restrictions on sensors and data transmission affect the quality and quantity of data collection. By reducing the powering burden of the propulsor, both applicability of UGs to oceanographic research and the quality of collected data will improve.

Dynamic modelling has proven to be a useful tool when assessing manoeuvrability, kinematic performance and energy performance for all AUVs. Leonard and Graver (2001) and Sagatun and Fossen (1991) developed the key framework for non-linear modelling of UGs and AUVs. And recent research conducted by Song et al. (2025) and Wang et al. (2025) has built upon this, providing in-depth research into modelling accuracy. Providing thorough energy consumption modelling and complex hydrological factors to accurately simulate real-world performance for UGs.

Dynamic models exist for a large quantity of different UG architectures, mass-variable systems have been modelled with success by Huang et al. (2021) and Tiwari and Sharma (2021). Volume-variable systems are commonplace, with a wide range of research in dynamic modelling, covering motion accuracy, path planning and energy performance (Liu et al., 2017; Song et al., 2025; Wu et al., 2021). However there is a lack of comparative study between UG architectures, and very little commentary on the performance differences between mass-variable and buoyancy-variable UGs. Often model derivations will make different assumptions, often utilise different modelling methodologies, this can skew comparison between two UG models. By modelling with consistent assumptions, a fair comparison between volume-variable and mass-variable underwater gliders can be made.

The findings from a fair comparison will highlight the differences between the two variable-buoyancy methods and their implications on the crucial limiting factors of UG operation in an oceanographic context, namely energy demand and manoeuvring performance. This can provide for more informed decision making regarding buoyancy engine choice in future UG design.

1.2 Research Aim

This project shall provide a novel comparative study of mass-variable and volume-variable UGs, in order to address the lack of comparison between the two variable buoyancy methods carried out in identical, fair and controlled tests.

Through the course of this paper, a non-linear, six degrees of freedom dynamic model will be proposed and used to assess the performance differences of mass-variable and volume-variable UGs in identical scenarios for a fair comparison. This paper excludes hydrological considerations such as currents, to provide a comparison in idealised conditions, in order to isolate differences with respect to dynamic behaviour.

By constructing this comparison, this paper aims to answer the following research questions:

1. How do the different variable buoyancy systems affect UG motion in ideal fluid conditions?
2. How do energy demands compare in common UG mission scenarios?
3. Does one system have beneficial energy consumption and manoeuvrability characteristics over the other?

2 Model Derivation

An underwater glider is a multi-body system, consisting of a hull and several subsystems that can be used to control motion during operation. By formulating the rigid-body Newton-Euler equations of motion, UG dynamics can be expressed mathematically, and subsequently simulated and assessed.

The following derivation follows the structure laid out by T. I. Fossen (2002) for marine vehicle dynamics. Expressed in the final form:

$$\begin{aligned} \boldsymbol{M}\dot{\boldsymbol{\nu}} + \boldsymbol{C}(\boldsymbol{\nu})\boldsymbol{\nu} + \cancel{\boldsymbol{D}(\boldsymbol{\nu})\boldsymbol{\nu}} &= \sum \boldsymbol{\tau}, \\ \dot{\boldsymbol{\eta}} &= \boldsymbol{J}(\boldsymbol{\eta})\boldsymbol{\nu} \end{aligned} \tag{1}$$

Where each term is defined as the following:

- $\boldsymbol{\nu}$ The body-fixed state vector: $\boldsymbol{\nu} = [u, v, w, p, q, r]^\top$
- $\boldsymbol{\eta}$ The NED-fixed position and Euler angles: $\boldsymbol{\eta} = [n, e, d, \phi, \theta, \psi]^\top$
- $\boldsymbol{J}(\boldsymbol{\eta})$ Transformation matrix for velocities in the body-fixed and NED-fixed frames.
- $\boldsymbol{M}$ The system inertia matrices, for both the rigid body and added mass: $\boldsymbol{M}_{RB} + \boldsymbol{M}_A$
- $\boldsymbol{C}(\boldsymbol{\nu})$ The system centripetal and Coriolis matrices, for both the rigid body and added mass: $\boldsymbol{C}_{RB} + \boldsymbol{C}_A$

- $\boldsymbol{D}(\boldsymbol{\nu})$ The hydrodynamic damping matrix, in this model it is not included as $\boldsymbol{\tau}_H$ accounts for all viscous effects.
- $\sum \boldsymbol{\tau}$ The sum of all control vectors, defined for each subsystem in **Section 2.2**.

2.1 The Reference Frames

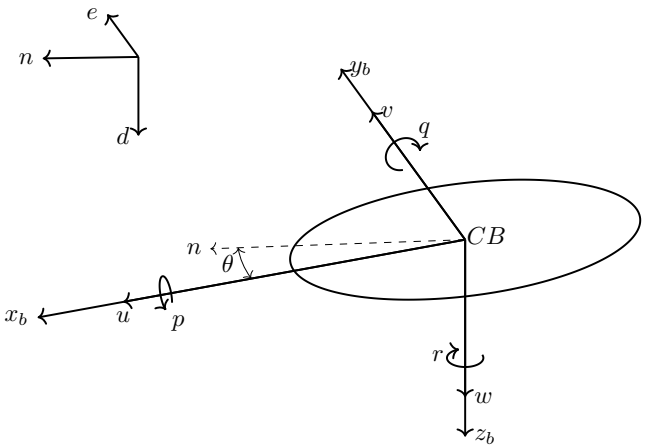


Figure 1: A figure detailing the body-fixed and NED-fixed frames, and body-fixed velocities

UG motion can be described in the body-fixed frame, this does not suffice for describing its position relative to earth. Thus both a body and earth fixed frame of reference is required. As is common with modelling of marine vehicles, the North-East-Down (NED) reference frame is chosen to describe the body's position.

The NED frame can be assumed to be inertial for vessels operating over a small local area relative to the Earth's surface. Transformation between body and NED fixed frames is achieved with three principle rotations about z, x and y. Linear velocities can be transformed from body-fixed to NED using the following rotational matrix:

$$\boldsymbol{R}_b^n(\boldsymbol{\Theta}) = \begin{bmatrix} \cos\psi\cos\theta & -\sin\psi\cos\phi + \cos\psi\sin\theta\sin\phi & \sin\psi\sin\phi + \cos\psi\cos\phi\sin\theta \\ \sin\psi\cos\theta & \cos\psi\cos\phi + \sin\phi\sin\theta\sin\psi & -\cos\psi\sin\phi + \sin\theta\sin\psi\cos\phi \\ -\sin\theta & \cos\theta\sin\phi & \cos\theta\cos\phi \end{bmatrix} \quad (2)$$

Transformation between NED and body-fixed frame is achieved with the transpose of the above matrix:

$$\boldsymbol{R}_n^b(\boldsymbol{\Theta}) = \boldsymbol{R}_b^{n\top}(\boldsymbol{\Theta}) \quad (3)$$

Angular velocities can be transformed similarly by introducing a transformation matrix, $\boldsymbol{T}_\Theta(\boldsymbol{\Theta})$, such that:

$$\boldsymbol{\omega}_{nb}^b = \begin{bmatrix} \dot\phi \\ 0 \\ 0 \end{bmatrix} + \boldsymbol{R}_{x,\phi}^\top \begin{bmatrix} 0 \\ \dot\theta \\ 0 \end{bmatrix} + \boldsymbol{R}_{x,\phi}^\top \boldsymbol{R}_{y,\theta}^\top \begin{bmatrix} 0 \\ 0 \\ \dot\psi \end{bmatrix} := \boldsymbol{T}_\Theta^{-1}(\boldsymbol{\Theta})\dot{\boldsymbol{\Theta}} \quad (4)$$

Hence:

$$\boldsymbol{T}_\Theta(\boldsymbol{\Theta}) = \begin{bmatrix} 1 & \sin\phi\tan\theta & \cos\phi\tan\theta \\ 0 & \cos\phi & -\sin\phi \\ 0 & \frac{\sin\phi}{\cos\theta} & \frac{\cos\phi}{\cos\theta} \end{bmatrix} \quad (5)$$

2.2 Subsystems

2.2.1 Initial Buoyancy

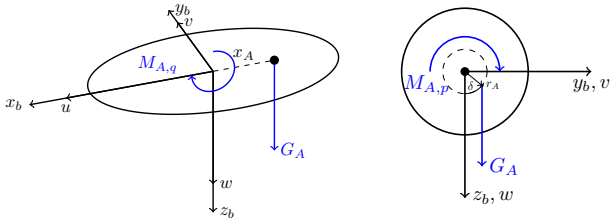
The origin of the body-fixed frame is assumed to be the centre of buoyancy of the glider. Naturally, the centre of gravity will be offset from the centre of buoyancy, Hence a restoring moment on the UG will occur. It is assumed that at an initial state, without a buoyancy engine, the UG will be neutrally buoyant. Therefore $G = B$ and the net force $\boldsymbol{f}_{GB} = [0, 0, 0]^\top$. The restoring moment, $\boldsymbol{m}_{GB}$ is calculated from the cross product of the body-fixed gravity force and the distance of the centre of gravity from origin:

$$\boldsymbol{m}_{GB} = \begin{bmatrix} x_G \\ y_G \\ z_G \end{bmatrix} \times \begin{bmatrix} -G\sin\theta \\ G\cos\theta\sin\phi \\ G\cos\theta\cos\phi \end{bmatrix} \quad (6)$$

The control vector representative of the initial buoyancy subsystem is expressed as:

$$\boldsymbol{\tau}_{GB} = \begin{bmatrix} \boldsymbol{f}_{GB} \\ \boldsymbol{m}_{GB} \end{bmatrix}, \boldsymbol{\tau}_{GB} \in \mathbb{R}^6 \quad (7)$$

2.2.2 Attitude Adjustment System



(a) Attitude adjustment (Pitching)

(b) Attitude adjustment (Rolling)

Figure 2: Figures detailing the Attitude adjustment system

Pitch and roll corrections are handled using a sliding and rotating mass. Pitch correction will behave similarly to the restoring moment, with a controlled offset fore or aft from the centre of buoyancy. Roll correction occurs from the mass rotating about the x_b axis to offset the gravity force from the moving mass vertically and transversely. It is assumed the moving mass has no net external force, so only moments are considered in the control vector, $\boldsymbol{\tau}_A$.

The lever arm for the moving mass is represented by:

$$\boldsymbol{r}_A = \begin{bmatrix} x_A \\ r_A\sin\delta \\ r_A\cos\delta \end{bmatrix} \quad (8)$$

Where x_A represents the longitudinal position of the mass, from the centre of buoyancy and δ represents the angle of rotation from z_b. The forces and moments are demonstrated for the sliding and rotating aspect of the adjustable mass in Figures 2(a) and 2(b) respectively.

The control vector representative of the attitude correcting mass is expressed as:

$$\boldsymbol{\tau}_A = \begin{bmatrix} 0 \\ 0 \\ 0 \\ G_A r_A\cos\theta(\sin\delta\cos\phi - \cos\delta\sin\phi) \\ -G_A(r_A\cos\delta\sin\theta + x_A\cos\theta\cos\phi) \\ G_A(x_A\cos\theta\sin\phi + r_A\sin\delta\sin\theta) \end{bmatrix} \quad (9)$$

2.2.3 Volume-Variable Buoyancy System

The volume-variable buoyancy system adjusts the volume of the UG, using an external bladder and internal reservoir filled with an incompressible fluid, such as oil. To allow for ascent or descent.

This model computes a change in buoyancy rather the absolute volume and its provided buoyancy, this way it can be assumed that when $\Delta B_B = 0$, the UG is neutrally buoyant, and the bladder is considered at 50% volume. This is a common approach when modelling the variable buoyancy subsystem for UGs (Jing et al., 2022; Wang et al., 2025).

It is assumed that the external bladder is symmetric in z_b and y_b, therefore the lever arm from ΔB_B is purely longitudinal. Hence the control vector for the variable-volume buoyancy system is given by:

$$\boldsymbol{\tau}_B = \begin{bmatrix} \Delta B_B \sin\theta \\ -\Delta B_B \cos\theta \sin\phi \\ -\Delta B_B \cos\theta \cos\phi \\ 0 \\ \Delta B_B x_B \cos\theta \cos\phi \\ -\Delta B_B x_B \cos\theta \sin\phi \end{bmatrix} \tag{10}$$

Where: $\Delta B_B = \rho_{sw} g \Delta V_B$, where ΔV_B is the volume change of the bladder.

2.2.4 Mass-Variable Buoyancy System

The mass-variable buoyancy system adjusts the mass of the UG, using an internal reservoir and pump to intake or expel fluid as ballast thus altering the mass of the glider to allow for ascent or descent. Similarly to the volume variable counterpart, a change in mass is computed rather than the absolute mass and its provided gravity force. Hence it can be assumed that when $\Delta G_B = 0$, the UG is neutrally buoyant and at 50% ballast. It is assumed that the internal ballast tank is symmetric in z_b and y_b, therefore the lever arm is purely longitudinal. The control vector for the variable-mass buoyancy system is given by:

$$\boldsymbol{\tau_M} = \begin{bmatrix} -\Delta G_B \sin\theta \\ \Delta G_B \cos\theta \sin\phi \\ \Delta G_B \cos\theta \cos\phi \\ 0 \\ -\Delta G_B x_B \cos\theta \cos\phi \\ \Delta G_B x_B \cos\theta \sin\phi \end{bmatrix} \tag{11}$$

Where: $\Delta G_B = \Delta m_B g$, where Δm_B is the mass change of the reservoir.

2.2.5 Viscous Hydrodynamics System

To produce forward motion, UGs must generate lift during ascent and descent. The forces for lift and drag are given by:

$$\begin{aligned} L &= \frac{1}{2}\rho A U^2 C_l \\ D &= \frac{1}{2}\rho A U^2 C_d \end{aligned} \tag{12}$$

Lift and drag do not act directly in the z_b and x_b axes inherently, by introducing stability and current axes (shown in Figure 3), lift and drag can be rotated to the body-fixed frame.

$$\begin{aligned} \boldsymbol{R}_{y,\alpha} &= \begin{bmatrix} \cos\alpha & 0 & \sin\alpha \\ 0 & 1 & 0 \\ -\sin\alpha & 0 & \cos\alpha \end{bmatrix} \\ \boldsymbol{R}_{z,-\beta} &= \begin{bmatrix} \cos\beta & \sin\beta & 0 \\ -\sin\beta & \cos\beta & 0 \\ 0 & 0 & 1 \end{bmatrix} \end{aligned} \tag{13}$$

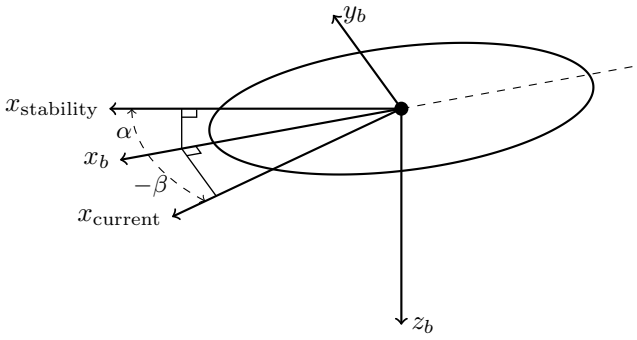


Figure 3: A figure detailing the introduced stability and current axes

By rotating by the above matrices, body-fixed viscous hydrodynamic forces can be resolved:

$$\boldsymbol{f}_H^b = \boldsymbol{R}_{y,\alpha}^\top \boldsymbol{R}_{z,-\beta}^\top \boldsymbol{f}_H^{\text{current}} \tag{14}$$

α and β can be determined with the same rotation, using the body-fixed velocities:

$$\begin{aligned} u &= U\cos\alpha\cos\beta \\ v &= U\sin\beta \\ w &= U\sin\alpha\cos\beta \end{aligned} \tag{15}$$

Where U is the resultant body-fixed velocity.

As recommended by T. I. Fossen (2002), modelling all viscous effects, including damping can be achieved in the same control vector. Hence the damping matrix, $\boldsymbol{D}(\boldsymbol{\nu})$ is neglected, as damping is accounted for with all other viscous effects.

Resolving the coefficients for the viscous forces and moments $(C_l, C_d, \ldots)$ would require either rigorous model testing or CFD for a given UG. That would be time consuming and deviate from the purpose of this research, hence viscous hydrodynamic coefficients have been taken from Wu et al. (2021), where CFD tests were carried out to calculate viscous hydrodynamic properties for the *PETREL-II* glider. The presented coefficients were given as dimensional values such that:

$$\boldsymbol{\tau}_H^{\text{current}} = \begin{bmatrix} \boldsymbol{f}_H^{\text{current}} \\ \boldsymbol{m}_H^{\text{current}} \end{bmatrix} = U^2 \begin{bmatrix} -K_{D0} - K_D\alpha^2 \\ K_\beta\beta \\ -K_{L0} - K_\alpha\alpha \\ K_{MR}\beta + K_p p \\ K_{M0} + K_M\alpha + K_q q \\ K_{MY}\beta + K_r r \end{bmatrix} \tag{16}$$

It was stated that, the above formulation is only valid when $u > 0$, Wu et al., 2021 provided a similar expression for negative forward body-fixed velocity. This would typically be applicable for when sea currents are modelled, Within the scope of this project, forward body-velocity will always be positive.

Other published coefficients for the *PETREL-II* were presented as non-dimensional values (Yang et al., 2017), and it was uncertain which values for the length or area dimensions should be used. To avoid this uncertainty when choosing values, the dimensional values from Wu et al. (2021) were chosen.

By rotating $\boldsymbol{\tau}_H^{\text{current}}$ by $\boldsymbol{R}_{y,\alpha}^\top \boldsymbol{R}_{z,-\beta}^\top$, the body-fixed control vector $\boldsymbol{\tau}_H$ can be computed.

2.3 Dynamic Model

2.3.1 Rigid Body EOMs

The rigid body system inertia and Coriolis matrices were derived from Kirchhoff's equations of motion, as established in Sagatun and Fossen (1991):

$$\boldsymbol{M}_{RB} = \begin{bmatrix} m & 0 & 0 & 0 & mz_g & -my_g \\ 0 & m & 0 & -mz_g & 0 & mx_g \\ 0 & 0 & m & my_g & -mx_g & 0 \\ 0 & -mz_g & my_g & I_x & -I_{xy} & -I_{xz} \\ mz_g & 0 & -mx_g & -I_{yx} & I_y & -I_{yz} \\ -my_g & mx_g & 0 & -I_{zx} & -I_{zy} & I_z \end{bmatrix} \tag{17}$$

Due to the approximate geometric symmetry of a UG, the off diagonal inertial terms can be neglected, $I_{xy} = I_{xz} = I_{yx} = I_{yz} = I_{zx} = I_{zy} = 0$. This assumption is common with UG modelling (Wang et al., 2025).

$\boldsymbol{C}_{RB}$ can be computed from the body-frame state vector, $\boldsymbol{\nu}$ and the mass and inertial values, this can be mapped simply due to its skew-symmetric nature: (T. Fossen & Fjellstad, 1995)

$$\boldsymbol{C}_{RB}(\boldsymbol{\nu}) = \begin{bmatrix} \boldsymbol{0}_{3\times3} & -m\boldsymbol{S}(\boldsymbol{\nu}_1) - m\boldsymbol{S}(\boldsymbol{\nu}_2)\boldsymbol{S}(\boldsymbol{r}_G^b) \\ -m\boldsymbol{S}(\boldsymbol{\nu}_1) + m\boldsymbol{S}(\boldsymbol{r}_G^b)\boldsymbol{S}(\boldsymbol{\nu}_2) & -\boldsymbol{S}(\boldsymbol{I}_G\boldsymbol{\nu}_2) \end{bmatrix} \tag{18}$$

Where:

$$\boldsymbol{S} = -\boldsymbol{S}^\top \tag{19}$$

$$\boldsymbol{S}\begin{bmatrix}\lambda_1\\ \lambda_2\\ \lambda_3\end{bmatrix} = \begin{bmatrix} 0 & -\lambda_3 & \lambda_2 \\ \lambda_3 & 0 & -\lambda_1 \\ -\lambda_2 & \lambda_1 & 0 \end{bmatrix} \tag{20}$$

And, $\boldsymbol{\nu}_1 = [u, v, w]^\top, \boldsymbol{\nu}_2 = [p, q, r]^\top$.

In the case of the variable-mass glider. Both the glider net mass and inertial properties of the glider will change as the internal quantity and distribution of mass changes. The new inertial properties of the glider for a given time-step can be found using parallel-axes theorem:

$$\boldsymbol{r} = \boldsymbol{r}_b - \frac{m_0\boldsymbol{r}_g + m_b(t)\boldsymbol{r}_b}{m(t)} \tag{21}$$

$$\boldsymbol{I}(t) = \boldsymbol{I}_0 + m_b(t)\left(\boldsymbol{r}^2\boldsymbol{I}_3 - \boldsymbol{r}\boldsymbol{r}^\top\right) \tag{22}$$

Where $m_0, m_b, m(t)$ are the initial glider mass, ballast mass and total mass respectively. $\boldsymbol{r}_g$ represents the distance from CB to CG for the glider in its initial state. r_b represents the distance from CB to the CG of the ballast tank. $\boldsymbol{I}_3$ denotes a 3×3 identity matrix.

Within this derivation, it is assumed that, provided the attitude adjusting mass has a small range of movement, it can be ignored from the derivation for the system inertia matrix. This aligns with the modelling assumptions of Wang et al. (2025). However in the model proposed by Rambech et al. (2025) it is considered, with a separate inertial matrix.

2.3.2 Added Mass

In addition to the rigid-body dynamics, UG motion induces motion of surrounding fluid, this contributes to the inertia of the system. By introducing added mass terms to the equations of motion, this effect can be accounted for. The contribution of added mass comes from the kinetic energy of the surrounding fluid: (Lamb, 1945)

$$T_A = \frac{1}{2}\boldsymbol{\nu}^\top\boldsymbol{M}_A\boldsymbol{\nu} \tag{23}$$

This follows the Lagrangian formulation for the rigid-body and fluid system proposed by Sagatun and Fossen (1991), who derived the added mass matrix, $\boldsymbol{M}_A$ from Kirchhoff's equations of motion:

$$\boldsymbol{M}_A = \begin{bmatrix} X_{\dot{u}} & X_{\dot{v}} & X_{\dot{w}} & X_{\dot{p}} & X_{\dot{q}} & X_{\dot{r}} \\ Y_{\dot{u}} & Y_{\dot{v}} & Y_{\dot{w}} & Y_{\dot{p}} & Y_{\dot{q}} & Y_{\dot{r}} \\ Z_{\dot{u}} & Z_{\dot{v}} & Z_{\dot{w}} & Z_{\dot{p}} & Z_{\dot{q}} & Z_{\dot{r}} \\ K_{\dot{u}} & K_{\dot{v}} & K_{\dot{w}} & K_{\dot{p}} & K_{\dot{q}} & K_{\dot{r}} \\ M_{\dot{u}} & M_{\dot{v}} & M_{\dot{w}} & M_{\dot{p}} & M_{\dot{q}} & M_{\dot{r}} \\ N_{\dot{u}} & N_{\dot{v}} & N_{\dot{w}} & N_{\dot{p}} & N_{\dot{q}} & N_{\dot{r}} \end{bmatrix} \tag{24}$$

Here SNAME (1950) notation for hydrodynamic derivatives is used for simplicity: $X_{\dot{u}} = \frac{\partial X}{\partial \dot{u}}$

It can be assumed that the UG has port-starboard symmetry and approximate top-bottom symmetry ($y = -y$, $z = -z$). This significantly simplifies the added mass matrix:

$$\boldsymbol{M}_A = \begin{bmatrix} X_{\dot{u}} & 0 & 0 & 0 & 0 & 0 \\ 0 & Y_{\dot{v}} & 0 & 0 & 0 & Y_{\dot{r}} \\ 0 & 0 & Z_{\dot{w}} & 0 & Z_{\dot{q}} & 0 \\ 0 & 0 & 0 & K_{\dot{p}} & 0 & 0 \\ 0 & 0 & M_{\dot{w}} & 0 & M_{\dot{q}} & 0 \\ 0 & N_{\dot{v}} & 0 & 0 & 0 & N_{\dot{r}} \end{bmatrix} \tag{25}$$

It is reasonable to assume that $\boldsymbol{M}_A$ is positive definite, which implies: $Z_{\dot{q}} = M_{\dot{w}}$ and $N_{\dot{v}} = Y_{\dot{r}}$. These assumptions align well with previous models proposed by Jing et al. (2022) and Wang et al. (2025).

Similarly to its rigid body counterpart, $\boldsymbol{C}_A$ can be computed simply, by exploiting its skew-symmetric nature, from $\boldsymbol{M}_A$:

$$\boldsymbol{C}_A = \begin{bmatrix} \boldsymbol{0}_{3\times3} & -\boldsymbol{S}(\boldsymbol{A}_{11}\boldsymbol{\nu}_1 + \boldsymbol{A}_{12}\boldsymbol{\nu}_2) \\ -\boldsymbol{S}(\boldsymbol{A}_{11}\boldsymbol{\nu}_1 + \boldsymbol{A}_{12}\boldsymbol{\nu}_2) & -\boldsymbol{S}(\boldsymbol{A}_{21}\boldsymbol{\nu}_1 + \boldsymbol{A}_{22}\boldsymbol{\nu}_2) \end{bmatrix} \tag{26}$$

Where:

$$\boldsymbol{M}_A = \begin{bmatrix} \boldsymbol{A}_{11} & \boldsymbol{A}_{12} \\ \boldsymbol{A}_{21} & \boldsymbol{A}_{22} \end{bmatrix} \tag{27}$$

3 Performance Metrics

3.1 Work Modelling

UGs can be divided into four energy consuming components: (Song et al., 2025)

1. The buoyancy engine
2. Attitude regulation system
3. Control-navigation-detection system
4. Communication system

For the purposes of this project, the latter two can be neglected. In the interest of maintaining a fair comparison, energy consumption modelling is done for an ideal condition, ignoring frictional and powering losses. This also means that only mechanical work demand is modelled, not electrical energy. This should be treated as an indicator of energy performance, and represents an upper bound, best-case scenario.

3.1.1 Variable Buoyancy System

As the earlier proposed equations of motion are solved numerically, time passes in discrete steps of a fixed size, within the model implementation additional computation can be done at each discrete point in time; this is exploited for a simple method of computing work over the course of a mission. The per time step work done against hydrostatic pressure, to achieve a mass or volume change,

for variable mass and buoyancy engines is given by the below equations respectively.

$$dW_B = d(t)\rho g|\Delta V_b| \tag{28}$$

$$dW_B = d(t)g|\Delta m_b| \tag{29}$$

Where $d(t)$ is the depth of the glider at the given time step. The total work done by the buoyancy engine over the course of a mission is then given by:

$$W_B = \sum^{t_{\max}} dW_B \tag{30}$$

3.1.2 Attitude Adjustment System

As previously established in **Section 2.2.2**, the position of the moving mass is given by $\boldsymbol{r}_A$, hence the work done against gravity per time step ($-z$ displacement of the block), by the moving mass can be found by:

$$dW_A = \max\left(m_A g(-1(\boldsymbol{R}\cdot\Delta\boldsymbol{r}_A), 0\right) \tag{31}$$

Where:

$$\boldsymbol{R} = [-\sin\theta, \sin\phi\cos\theta, \cos\phi\cos\theta] \tag{32}$$

This rotates the displacement of the block, including only the z-axis displacement, as no work is done against gravity in y or x-axis. It is assumed that the attitude adjustment system is non regenerative, therefore work done by gravity to move the mass block is lost. Hence values such that $dW_A < 0$ are discounted. Similarly to the work computation for the variable buoyancy systems, the per time step work for the attitude adjustment system is summated over the course of a mission to provide the total work done by the attitude adjustment system: W_A.

4 Simulation and Model Implementation

The proposed model was implemented in `MATLAB`, with a simple control system, following Leonard and Graver (2001), where desired velocity and path angle are set. The sliding mass and buoyancy engine are adjusted to reduce the error between the desired velocity and pitch angle and the values experienced by the glider at that time.

In a sawtooth mission profile, target parameters for depth, pitch and body-fixed down velocity are set. When the target depth is met, the target pitch and velocity will invert, to begin ascent. To avoid hysteresis a small band value is defined, to encourage transition just before the target. To avoid chattering, the glider is to maintain its target pitch and velocity between the upper and lower target depths.

The target pitch and velocity values are defined as θ_{sp} and w_{sp} respectively, at every step in the simulation, an error value is computed using the current pitch and velocity:

$$\begin{aligned} \theta_e &= \theta_{sp} - \theta \\ w_e &= w_{sp} - w \end{aligned} \tag{33}$$

By multiplying the error values by a fixed gain value, the commanded change for the buoyancy engine and attitude adjustment block can be found. During the simulations carried out in this project, for the sake of a fair comparison, the gain values were the same for both the variable mass and variable volume systems.

The change prescribed by the gain-multiplied error value may result in unrealistic and rapid changes to the buoyancy engine and attitude adjustment block, because of this, an actuator is in place. This limits the change according to the maximum rate of change and the upper and lower bounds of each system respectively. The actuator limited change to the buoyancy engine and attitude adjustment block is applied to the system for a more realistic transition and adjustment.

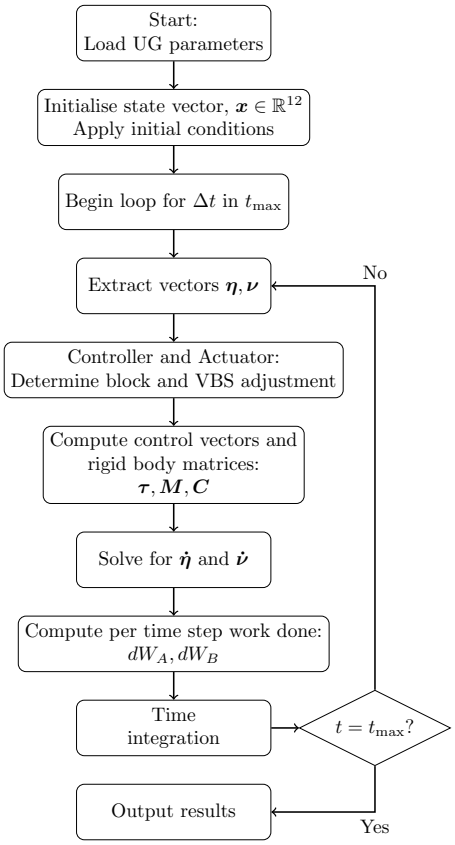


Figure 4: A flowchart detailing the model implementation in `MATLAB`

For missions where sway and yaw require commanding, an additional parameter was made to set a desired roll angle, ϕ_{sp}, for which the error value can be similarly found by:

$$\phi_e = \phi_{sp} - \phi \tag{34}$$

A gain value and actuator limit is similarly applied to this component of the attitude adjustment.

The discrete state derivatives for each time step, $\dot{\boldsymbol{\nu}}, \dot{\boldsymbol{\eta}}$ were integrated numerically using a 4^{th} order Runge-Kutta scheme. For a suitable simulation accuracy, a reasonably small time-step was chosen: $\Delta t = 0.02s$.

Figure 4, demonstrates the model implementation with a simple flowchart.

5 UG Parameters

As previously mentioned, model testing and calculating UG parameters and hydrodynamic derivatives is beyond the scope of this research, therefore published data was used for all parameters that define the glider geometry and hydrodynamic properties. For this research the *PETREL-II* glider was chosen, as published testing data and parameters are readily available. For the purposes of a comparative study between mass and volume-variable UGs, all parameters excluding those relevant to the buoyancy systems should be the same between the two implementations. Tables 1, 2, 3 and 4

list the parameters used in the model implementation.

Table 1: Glider Physical Parameters (Wang et al., 2025)

Parameter	Value	Unit
Glider mass, m	57	kg
Glider length, L	1.97	m
Glider characteristic area, A_D	0.038	m^2
Moment of Inertia, I_{xx}, I_{yy}, I_{zz}	$0.54, 17.75, 17.75$	$kg\,m^2$
CG	$[0, 0, 0.06]^\top$	m
Sliding block mass, m_A	17.3	kg
Sliding block loci, r_A	0.1	m

Table 2: Added Mass Parameters (Wang et al., 2025)

Parameter	Value	Unit
$X_{\dot{u}}$	1.25	kg
$Y_{\dot{v}}$	58.1	kg
$Z_{\dot{w}}$	61.25	kg
$K_{\dot{p}}$	0	$kg\,m^2$
$M_{\dot{q}}$	10.57	$kg\,m^2$
$N_{\dot{r}}$	10.58	$kg\,m^2$
$Y_{\dot{r}}$	0.614	$kg\,m$
$Z_{\dot{q}}$	0.45	$kg\,m$

Table 3: Viscous Hydrodynamic Parameters (Wu et al., 2021)

Parameter	Value	Unit
K_{D0}	7.65	$kg\,m^{-1}$
K_D	357.97	$kg\,m^{-1}\,rad^{-2}$
K_β	-100.13	$kg\,m^{-1}\,rad^{-1}$
K_{L0}	-0.5	$kg\,m^{-1}$
K_α	381.73	$kg\,m^{-1}\,rad^{-1}$
K_{MR}	-55.81	$kg\,rad^{-1}$
K_p	-18.98	$kg\,s\,rad^{-1}$
K_{M0}	0.3	kg
K_M	-61.02	$kg\,rad^{-1}$
K_q	-196.78	$kg\,s\,rad^{-1}$
K_{MY}	32.63	$kg\,rad^{-1}$
K_r	-372.54	$kg\,s\,rad^{-1}$

Table 4: Actuator and Gain Parameters

Parameter	Value	Unit
Sliding Mass Aft Limit	-0.16	m
Sliding Mass Fore Limit	0.54	m
Sliding Mass Speed	0.001	ms^{-1}
Mass Rotation Speed	0.035	$rad\,s^{-1}$
Ballast & Bladder limits	± 0.5	kg
Ballast Flow Rate	0.0077	$kg\,s^{-1}$
Pump Rate	$1.7e-6$	$m^3 s^{-1}$
Solenoid Rate	$7.5e-6$	$m^3 s^{-1}$
Gain: w	90	-
Gain: θ	1	-
Gain: ϕ	0.05	-

6 Model Validation

As referenced above, the parameters for testing were chosen to replicate the dynamics of the *PETREL-II* UG, this is due to the large quantity of published model and sea-trial data, for various scenarios and manoeuvres. However, due to the fact the *PETREL-II* is highly configurable for different payloads or mission conditions, the parameters will vary from instance to instance. This makes validating by direct comparison difficult, as many papers do not include all of the required parameters for the simulations. Furthermore, most current UG implementations, with published data, including the *PETREL-II* are volume-variable. Meaning that validation for the mass-variable model by means of comparison to published data is not practical.

By commanding a pitch angle, θ of $\pm 40°$ for a sawtooth-like scenario, with a target depth of $900m$. The dynamic motion of the volume variable UG model can be compared to that of Wang et al. (2025). It is important to note, that this model does not include hydrological or environmental effects, such as currents, buoyancy loss from hull deformation or variable seawater density. Hence results between the proposed model, and that published by Wang et al. (2025) will differ.

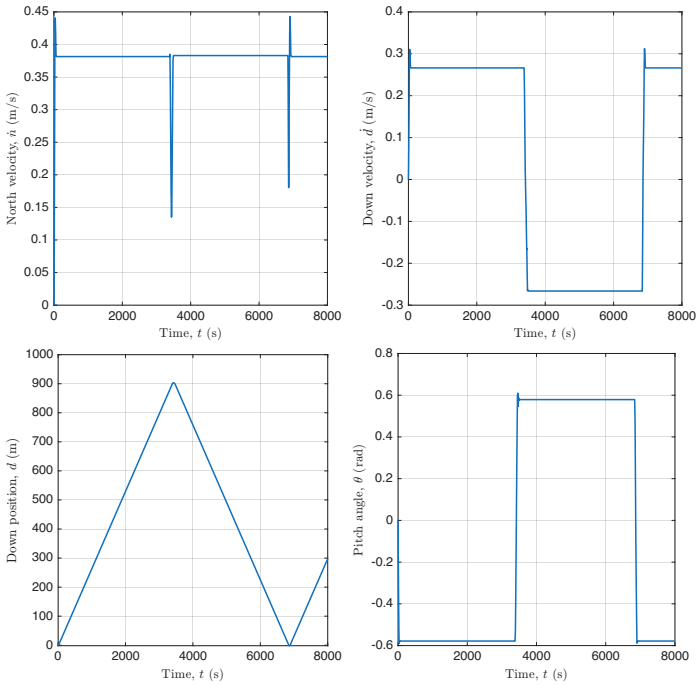


Figure 5: Results from the described $\pm 40°$ pitch sawtooth profile over time, $t\,(s)$

As expected, the results do not align exactly with those found by Wang et al. (2025), however they do demonstrate expected UG motion, for a still water environment with no hydrological considerations and constant seawater density, $\rho = 1025kg\,m^{-3}$. As shown in Figure 5: the achieved pitch angle is also lower than the commanded pitch angle, this is expected, as the pitch angle is limited by the stroke of the sliding mass, restoring and hydrodynamic moments. The velocities plotted are greater in magnitude to those found by Wang et al. (2025), this is expected as the omitted environmental effects would reduce the UG's velocities; Wang et al. (2025) found that buoyancy loss particularly, causes a reduction in vertical velocity. With their testing demonstrating a reduction from $0.18ms^{-1}$ to $0.12ms^{-1}$ at a $700m$ depth. This also explains the faster completion time exhibited, to perform the dive and climb to and from a $900m$ depth. The recorded North velocity is $0.065ms^{-1}$ higher than that found by Wang et al. (2025), during steady gliding. Hydrological effects are said not to impact horizontal velocity significantly. Therefore, this is most likely explained by the use of different viscous hydrodynamic parameters. The proposed model in ideal fluid conditions, represents an upper

bound for UG motion and energy performance, and is suitable for a comparative study between mass and volume-variable UGs.

Full validation beyond simply confirming motion is achieved as expected, would require experimental testing or sea trials, which is beyond the scope of this research.

Whilst the found results from the proposed model implementation do not agree fully with those found by Wang et al. (2025), this was expected and does not undermine the usability of the model implementation as a means of achieving the research goals within this project. Differences between numerical models are normal, with discrepancies arising from different numerical schemes and modelling assumptions. However the proposed model does present behaviour expected for ideal conditions during the tests, discrepancies relating to vertical velocity are physically consistent with the omission of hydrological effects. Importantly, this model does not aim to replicate real UG performance in an ocean environment, but to provide a fair and internally consistent comparison between mass-variable and volume-variable UGs in ideal conditions. As the two UG implementations share the same parameters, modelling assumptions and numerical scheme, any errors introduced by modelling simplifications will affect both equally, and will not bias the comparative results. Hence the model implementations are of sufficient accuracy for an initial answer to the research aims of this project, as long as findings are made in a comparative context between the two architectures and the model limitations are acknowledged.

7 Simulation Results

7.1 Performance in a Sawtooth Profile

To assess the energy performance of the two types of UG, a batch of sawtooth tests were performed at varying commanded pitch angles. This was chosen, as the pitch angle is one of the few operationally modifiable variables, and the sawtooth profile is the most popular for UG operation. As UG velocity is not consistent between the ranges of pitch and the types of variable buoyancy system (VBS), work done by the VBS and attitude regulation systems is recorded until an achieved distance in the North direction. A target depth of $1000m$ and $10000m$ Northing was chosen to represent a possible mission scenario where a UG may be used in oceanographic research (Rudnick et al., 2004). Often UGs will cover far greater distances, but in order to maintain a reasonable simulation run-time at a reasonably small time-step, the Northing distance was kept low, whilst still allowing for multiple sawtooth cycles. The trajectories of the UGs during this test are displayed in Figure 6.

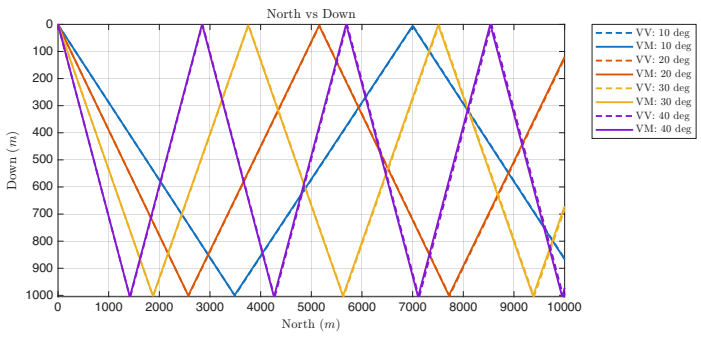


Figure 6: Trajectories of both type of UG at a range of pitch angles

Table 5 and Table 6 present the ideal energy consumption of the variable-volume and variable-mass gliders respectively, using the earlier described method (**Section 3.1**) for the range of commanded pitch angles as shown in Figure 6.

Table 5: Results from the $10000m$ Northing mission for the variable-volume system

Pitch angle, $\theta\,(^\circ)$	**Time to complete,** (s)	**VBS consumption,** (J)	**Attitude Adjust consumption,** (J)
10	31396	9871.6	1272.3
20	24333	19682	67.06
30	21700	29551	78.45
40	20897	39359	107.17

Table 6: Results from the $10000m$ Northing mission for the variable-mass system

Pitch angle, $\theta\,(^\circ)$	**Time to complete,** (s)	**VBS consumption,** (J)	**Attitude Adjust consumption,** (J)
10	31325	9860.6	1257.8
20	24182	19668	36.8
30	21493	29537	26.1
40	20672	39409	45.1

As previously mentioned, the delivered pitch angle and commanded pitch angle differ. However, as indicated by the lowered energy consumption of the attitude adjustment subsystem for $\theta > 10$ for both variable-mass and volume systems, a steady glide angle is not achieved at the low angle of commanded pitch. This is also demonstrated graphically by Figure 7, where pitch angle fluctuates consistently between the diving and climbing transitions for $\theta = 10^\circ$. At lower pitch angles, the sliding mass block is expected to move less to achieve the desired pitch angle, however as the gain value for controlling pitch is set, to be appropriate for the larger pitch angles. This means the sliding mass will have a larger displacement than required, causing an overshoot, which is then attempted to be corrected. This causes the fluctuations at a desired pitch angle of 10°. A more sophisticated control system, with variable gain may prevent the exhibited fluctuations in pitch. However design and optimisation of such a control system is beyond the scope of this research project, and as the same instability is seen with both UG models, it should not harm the validity of the comparison.

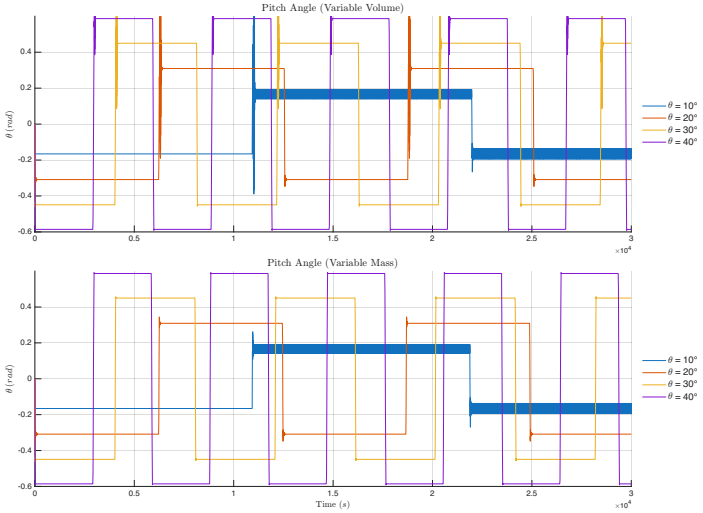


Figure 7: Pitch Angles during Sawtooth Test

The performance in the Sawtooth profile is similar for both UGs.

With the mass-variable UG exhibiting a minor improvement in completion time (-0.22 to -1.09%). The VBS work for both systems is near similar with differences ranging from -0.11 to 0.13%. This similarity was expected as both systems had the same capacity for the ballast tank and oil bladder respectively, with identical control parameters. As both systems do work against the same hydrostatic pressure, for the same net buoyancy change, the difference between them comes from how the rigid body dynamics are treated, not the work done to the bladder or tank to achieve a buoyancy change. The attitude adjustment work differed the most between the two systems, when excluding the unsteady gliding at $\theta = 10°$, the mass-variable UG experienced an 82.2 to 200.6% reduction in work for the attitude adjustment system.

The different, state-dependent rigid body properties of the mass-variable glider, likely contribute to this edge in attitude adjustment work. Adding internal ballast shifts the position of CG further from CB, which in turn increases the restoring moment that contributes to pitch, requiring less attitude adjustment work to cause an adjustment to a desired pitch angle.

7.2 Manoeuvring Performance in Spiral Motion

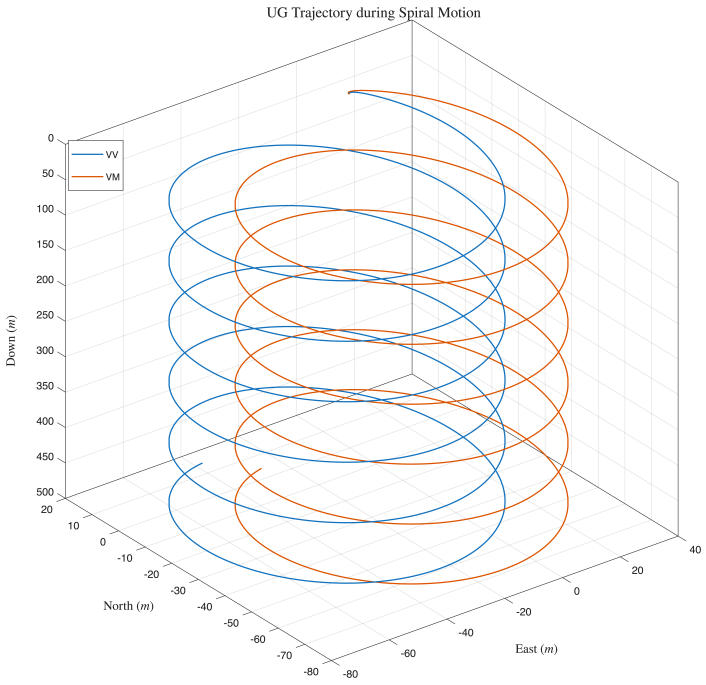


Figure 8: Spiral Motion Testing for both types of UG

A spiral test can demonstrate UG dynamics in six degrees of freedom and highlights the lateral aspects of UG motion, including rolling, yaw and sway. Which are not assessed in the sawtooth profile. Operationally, helical motion can be utilised to change the direction of a UG underwater (Zhang et al., 2013), or for station keeping near to a target in weak currents. (Clark et al., 2020)

The spiral motion was carried out by a fixed buoyancy engine and attitude adjustment, as to highlight manoeuvring differences between the two UGs. The attitude adjustment mass was fixed $0.02m$ forward and positioned, $\delta = 40°$ to cause a turn. The ballast tank and oil bladder were at 100% and 0% volume respectively. The UGs descended to $500m$ in a helical path from rest at the surface. The trajectories of both mass-variable and volume-variable UGs are shown in Figure 8. As expected, both UGs experienced similar helical glide trajectories, with identical descent. However the mass-variable UG experiences less bank overshoot whilst approaching a steady glide, and has a cleaner entry into the helical glide. The radius of the helical glide was marginally tighter for the mass-variable UG.

Both UGs approach a roll angle, $\phi = 1.914°$ during the steady turn. Prior to entry into the steady turn, the mass-variable UG experiences a maximum roll angle of $5.651°$ and the volume-variable UG experiences a maximum roll angle of $8.442°$.

The cleaner entry into steady glide exhibited by the mass-variable glider is likely due to the improved damping as a result of the internal ballast and its effect on the roll moment of inertia. This aligns with the reduced attitude adjustment work in the previous sawtooth test.

7.3 Limitations of the Model Results

As all simulations were done in ideal conditions, hydrological effects were not considered. Wang et al. (2025) proposed models for buoyancy loss due to hull deformation, variable seawater density and ocean currents to more accurately model UG motion in an ocean environment. In both simulation results and sea-trials, Wang et al. (2025) found that the hydrological effects will reduce vertical velocity and delay transitions between steady glides.

The earlier proposed energy modelling approach deliberately ignores frictional and powertrain losses and time based hotel loads, such as those from controllers or communication systems. To attempt to simplify the computation whilst still providing a fair comparison. However sophisticated energy consumption models proposed by Hu et al. (2023) and Song et al. (2021) consider a greater number of energy consuming factors over the course of a UG mission, including the controller and communication unit. The proposed energy consumption models are environmentally aware and consider electrical energy, and consider possible asymmetry in consumption between ascent and descent actions. These considerations will yield more meaningful results when considering and predicting UG energy performance in real-world use-cases, and could highlight a greater number of differences in operation between mass-variable and volume-variable UGs.

As our current simulations neglect hydrological influences, the results will overestimate the UG manoeuvring performance, especially the UGs ability to conform to controller authority. The simulations underestimate the required energy to complete the prescribed missions, as this model considers the work required, not the electrical energy, which is more meaningful when assessing the feasibility of a UG design to a mission scenario. Therefore these findings are considered an idealised best-case scenario, when comparing the two UGs. Future work should aim to incorporate more in-depth energy modelling and hydrological considerations, whilst maintaining a fair and balanced comparison.

8 Discussion

This section elaborates further on the simulation results and discusses their implications for future glider design and operation, structured using the research questions stated earlier.

From the sawtooth profile results in idealised fluid conditions, both UGs exhibit near identical steady state gliding motion. The mass-variable system experiences a negligible gain in velocity in North and Down, as demonstrated by the marginally lower completion times, when reaching a northing target. Even in idealised fluid conditions, the commanded pitch angle is not met during steady gliding, for either UG model, due to the limited stroke of the sliding mass, restoring and hydrodynamic moments. From this viewpoint neither variable buoyancy method provides a benefit over the other in the context of UG motion in ideal fluid conditions.

The trajectories exhibited in spiral motion testing are likewise very similar between the two UGs. The steady glide trajectories are near identical. The differences between the two variable buoyancy architectures is more significant in the transient state between rest and the start of the steady glide. As found in the spiral motion test, the mass-variable glider enjoyed a lower bank overshoot than the volume-variable counterpart, this is found from the lower maximum roll angle prior to the steady glide. This implies that the mass-variable UG will have cleaner entry into a spiral manoeuvre than the volume-variable UG. This is a result of the increased roll inertia from the internal ballast, which improves roll damping. In an operational context, this may result in improved station-keeping and responsiveness from rest.

In terms of energy consumption, both variable-mass and variable-volume UGs had similar results. The differences in work done by the variable buoyancy systems is negligible. However the variable-mass UG did enjoy lowered attitude adjustment work during the sawtooth missions. This is a result of the shifting CG due to the internal ballast, which in turn changes the restoring moment, which assists with pitching, reducing the demand for sliding block adjustment. Overall, however, this did not contribute to a significant loss in energy consumption.

However, as this study did not consider frictional losses or energy consumption from controllers, this difference may become more significant in reality. A more sophisticated energy modelling approach may result in more meaningful or insightful comparison between the two UGs and their performance concerning energy consumption.

As stated, the mass-variable UG has marginally improved performance over the volume-variable UG in the two tests. However the model limitations stated may impact the credibility and significance of the aforementioned findings.

9 Concluding Remarks

This study has found scenarios where a mass-variable UG outperforms a volume-variable UG, with identical parameters. Such as the reduced attitude adjustment work during sawtooth diving and climbing routines, where the mass-variable UG had a 82.2 to 200.6% reduction. Additionally, the mass-variable UG was found to have a more stable entry into steady, helical glides, with a lower banked overshoot. However, completion times between the two UGs were near identical, suggesting that the improved performance in entering spiral turns is only a benefit for station-keeping or virtual mooring exercises. The mass-variable glider, does not have an inherently faster descent.

As this study only looked at results in ideal fluid conditions, with rudimentary energy modelling; which ignored hotel loads, frictional and powertrain losses, and electrical energy, future work could endeavour to continue this comparative study with fewer limitations. This could involve stronger model validation, with model testing or sea trials. Additionally, in depth modelling of the ocean environment could enhance the comparative study and its applicability to real world UG missions. More sophisticated energy modelling would provide greater detail into the energy performance differences between the two UGs, this would assist in providing a more credible answer to the second research question.

Acknowledgement

I would like to thank Dr. Andrew Aspden for his advice and guidance throughout the course of this study. I would additionally like to thank Dr. David Trodden, for his feedback provided for the initial draft.

References

Carneiro, J. F., Pinto, J. B., de Almeida, F. G., & Cruz, N. A. (2024). Depth control of an underwater sensor platform: Comparison between variable buoyancy and propeller actuated devices. *Sensors*, *24*(10). https://doi.org/10.3390/s24103050

Clark, E. B., Branch, A., Chien, S., Mirza, F., Farrara, J. D., Chao, Y., Fratantoni, D., Aragon, D., Schofield, O., Flexas, M. M., & Thompson, A. (2020). Station-keeping underwater gliders using a predictive ocean circulation model and applications to swot calibration and validation. *IEEE Journal of Oceanic Engineering*, *45*(2), 371–384. https://doi.org/10.1109/JOE.2018.2886092

Fossen, T., & Fjellstad, O. E. (1995). Nonlinear modelling of marine vehicles in 6 degrees of freedom. *Mathematical Modelling of Systems*, *1*. https://doi.org/10.1080/13873959508837004

Fossen, T. I. (2002). Marine control systems : Guidance, navigation and control of ships, rigs and underwater vehicles.

Hu, H., Zhang, Z., Li, L., & Peng, X. (2023). Energy-optimal motion planning of underwater gliders accounting for seabed topography and ocean currents. *Ocean Engineering*, *288*, 116008. https://doi.org/10.1016/j.oceaneng.2023.116008

Huang, J., Choi, H.-S., Jung, D.-W., Lee, J.-H., Kim, M.-J., Choo, K.-B., Cho, H.-J., & Jin, H.-S. (2021). Design and motion simulation of an underwater glider in the vertical plane. *Applied Sciences*, *11*(17). https://doi.org/10.3390/app11178212

Jing, G., Lei, L., & Gang, Y. (2022). Dynamic modeling and experimental analysis of an underwater glider in the ocean. *Applied Mathematical Modelling*, *108*, 392–407. https://doi.org/https://doi.org/10.1016/j.apm.2022.03.034

Lamb, H. (1945). Hydrodynamics (6th ed.).

Leonard, N. E., & Graver, J. G. (2001). Model-based feedback control of autonomous underwater gliders. *IEEE Journal of Oceanic Engineering*, *26*(4), 633–645. https://doi.org/10.1109/48.972106

Liu, F., Wang, Y.-h., Wu, Z.-l., & Wang, S.-x. (2017). Motion analysis and trials of the deep sea hybrid underwater glider petrel-ii. *China Ocean Engineering*, *31*(1), 55–62. https://doi.org/10.1007/s13344-017-0007-4

Phillips, A. B., Haroutunian, M., Man, S. K., Murphy, A. J., Boyd, S. W., Blake, J. I. R., & Griffiths, G. (2012). Nature in engineering for monitoring the oceans: Comparison of the energetic costs of marine animals and auvs. In G. N. Roberts & R. Sutton (Eds.), *Further advances in unmanned marine vehicles* (pp. 373–405). Institution of Engineering; Technology. https://doi.org/10.1049/PBCE077E_ch17

Rambech, A. B., Saksvik, I. B., & Hassani, V. (2025). Combining moving mass actuators and manoeuvring models for underwater vehicles: A lagrangian approach. *IFAC-PapersOnLine*, *59*(22), 243–247. https://doi.org/https://doi.org/10.1016/j.ifacol.2025.11.639

Rudnick, D., Davis, R., Eriksen, C., Fratantoni, D., & Perry, M. J. (2004). Underwater gliders for ocean research. *Marine Technology Society Journal*, *38*, 73–84. https://doi.org/10.4031/002533204787522703

Sagatun, S. I., & Fossen, T. I. (1991). *Lagrangian formulation of underwater vehicles' dynamics*. https://doi.org/10.1109/ICSMC.1991.169823

SNAME. (1950). *Nomenclature for treating the motion of a submerged body through a fluid: Report of the american towing tank conference*. Society of Naval Architects; Marine Engineers.

Song, Y., Niu, W., Shi, W., Wu, H., & Xu, Y. (2025). Optimal feedback control parameters for underwater gliders: Balancing energy efficiency and motion accuracy. *Ocean Engineering*, *322*, 120544. https://doi.org/10.1016/j.oceaneng.2025.120544

Song, Y., Ye, H., Wang, Y., Niu, W., Wan, X., & Wei, M. (2021). Energy consumption modeling for underwater gliders considering ocean currents and seawater density variation. *Journal of Marine Science and Engineering*, *9*, 1164. https://doi.org/10.3390/jmse9111164

Stommel, H. (1989). The slocum mission. *Oceanography*, *2*(1), 22–25.

Tiwari, B., & Sharma, R. (2021). Study on system design and integration of variable buoyancy systems for underwater operation. *Defence Science Journal*, *71*, 124–133. https://doi.org/10.14429/dsj.71.15557

Wang, H., Wang, C., & Li, Y. (2025). Dynamic modeling and analysis of underwater glider in the ocean environment. *Ocean Engineering*, *332*, 121312. https://doi.org/https://doi.org/10.1016/j.oceaneng.2025.121312

Wu, H., Niu, W., Wang, S., & Yan, S. (2021). An optimization method for control parameters of underwater gliders considering energy consumption and motion accuracy. *Applied Mathematical Modelling*, *90*, 1099–1119. https://doi.org/https://doi.org/10.1016/j.apm.2020.10.015

Yang, Y., Liu, Y., Wang, Y., Zhang, H., & Zhang, L. (2017). Dynamic modeling and motion control strategy for deep-sea hybrid-driven underwater gliders considering hull deformation and seawater density variation. *Ocean Engineering*, *143*, 66–78. https://doi.org/https://doi.org/10.1016/j.oceaneng.2017.07.047

Zhang, S., Yu, J., Zhang, A., & Zhang, F. (2013). Spiraling motion of underwater gliders: Modeling, analysis, and experimental results. *Ocean Engineering*, *60*, 1–13. https://doi.org/https://doi.org/10.1016/j.oceaneng.2012.12.023

Appendices

A Nomenclature

A.1 Vectorial Quantities

North-East-Down (NED) Position:

$$\boldsymbol{p}^n = \begin{bmatrix} n \\ e \\ d \end{bmatrix}$$

Attitude (Euler angles):

$$\boldsymbol{\Theta} = \begin{bmatrix} \phi \\ \theta \\ \psi \end{bmatrix}$$

Body-fixed linear velocity:

$$\boldsymbol{v}_o^b = \begin{bmatrix} u \\ v \\ w \end{bmatrix}$$

Body-fixed angular velocity:

$$\boldsymbol{\omega}_{nb}^b = \begin{bmatrix} p \\ q \\ r \end{bmatrix}$$

Body-fixed force:

$$\boldsymbol{f}_o^b = \begin{bmatrix} X \\ Y \\ Z \end{bmatrix}$$

Body-fixed moment:

$$\boldsymbol{m}_o^b = \begin{bmatrix} K \\ M \\ N \end{bmatrix}$$

Control vectors:

$$\boldsymbol{\tau}^b = \begin{bmatrix} \boldsymbol{f}^b \\ \boldsymbol{m}^b \end{bmatrix}$$

Body-fixed state or Velocity vector:

$$\boldsymbol{\nu} = \begin{bmatrix} \boldsymbol{v}^b \\ \boldsymbol{\omega}^b \end{bmatrix}$$

NED-fixed Position vector:

$$\boldsymbol{\eta} = \begin{bmatrix} \boldsymbol{p}^n \\ \boldsymbol{\Theta} \end{bmatrix}$$

A.2 Symbols

$\boldsymbol{M}$	Total inertia matrix (rigid-body + added mass), $\mathbf{M} = \mathbf{M}_{RB} + \mathbf{M}_A$.
$\boldsymbol{C}(\boldsymbol{\nu})$	Total Coriolis/centripetal matrix (rigid-body + added mass), $\mathbf{C} = \mathbf{C}_{RB} + \mathbf{C}_A$.
$\boldsymbol{D}(\boldsymbol{\nu})$	Hydrodynamic damping matrix (neglected here; viscous effects are captured via $\boldsymbol{\tau}_H$).
$\boldsymbol{\tau}$	Total applied force-moment control vector (sum of subsystem contributions), $\boldsymbol{\tau} \in \mathbb{R}^6$.
$\boldsymbol{J}(\eta)$	Kinematic transformation mapping body-fixed velocities to NED rates.
ϕ, θ, ψ	Roll, pitch, yaw Euler angles (rad).
$\dot{\phi}, \dot{\theta}, \dot{\psi}$	Euler angle rates (rad s^{-1}).
$\boldsymbol{R}_b^n(\boldsymbol{\Theta})$	Rotation matrix from body frame b to NED frame n.
$\boldsymbol{R}_n^b(\boldsymbol{\Theta})$	Rotation matrix from NED frame n to body frame b, $\boldsymbol{R}_n^b = (\boldsymbol{R}_b^n)^\top$.
$\boldsymbol{T}_\Theta(\boldsymbol{\Theta})$	Euler-rate transformation matrix relating $\dot{\boldsymbol{\Theta}}$ and body angular velocity.
CB	Centre of buoyancy (chosen as body-frame origin).
CG	Centre of gravity.
G	Weight magnitude of the vehicle, $G = mg$ (N).
B	Buoyancy force magnitude (N).
x_G, y_G, z_G	Components of the CG location relative to CB, expressed in the body frame (m).
$\boldsymbol{\tau}_{GB}$	Hydrostatic subsystem contribution to the force-moment vector.
m_A	Sliding/rotating (attitude adjustment) mass (kg).
G_A	Weight magnitude of the attitude mass, $G_A = m_A g$ (N).
x_A	Longitudinal position of the attitude mass relative to CB (m).
r_A	Lever-arm radius of the rotating attitude mass about x_b (m).
δ	Rotation angle of the attitude mass about x_b (rad).
$\boldsymbol{r}_A$	Lever-arm vector from CB to the attitude mass CG (m).
$\boldsymbol{\tau}_A$	Attitude adjustment subsystem contribution to the force-moment vector.
x_B	Longitudinal lever arm of buoyancy/ballast actuation relative to CB (m).
ΔB_B	Change in buoyancy generated by the volume-variable system (N).
ΔV_B	Bladder volume change (m^3).
$\boldsymbol{\tau}_B$	Volume-variable buoyancy subsystem contribution to the force-moment vector.
ΔG_B	Change in weight generated by the mass-variable system (N).
Δm_B	Ballast mass change (kg).
$\boldsymbol{\tau}_M$	Mass-variable buoyancy subsystem contribution to the force-moment vector.
ρ_{sw}	Seawater density used in buoyancy change calculation (kg m^{-3}).
g	Acceleration due to gravity (m s^{-2}).

L	Lift force magnitude (N).
D	Drag force magnitude (N).
ρ	Fluid density (kg m^{-3}).
A	Reference/characteristic area used for lift/drag (m^2).
C_l, C_d	Lift and drag coefficients (non-dimensional).
U	Resultant body-fixed speed.
α	Angle of attack (rad).
β	Sideslip angle (rad).
$\boldsymbol{R}_{y,\alpha}$	Rotation matrix for angle of attack about the y-axis.
$\boldsymbol{R}_{z,-\beta}$	Rotation matrix for sideslip about the z-axis.
$\boldsymbol{\tau}_H^{\text{current}}$	Hydrodynamic viscous force-moment vector in the current/stability axes.
$\boldsymbol{\tau}_H$	Hydrodynamic viscous force-moment vector resolved in the body frame.
K_{D0}	
K_D	
K_β	
K_{L0}	
K_α	
K_{MR}	
K_p	Viscous hydrodynamic coefficients where the subscript denotes the relevant component of damping, lift or drag.
K_{M0}	
K_M	
K_q	
K_{MY}	
K_r	
$\boldsymbol{M}_{RB}$	Rigid-body inertia matrix.
$\boldsymbol{C}_{RB}$	Rigid-body Coriolis/centripetal matrix.
I_{xx}, I_{yy}, I_{zz}	Principal moments of inertia about body axes (kg m^2).
I_{xy}, I_{xz}, I_{yz}	Products of inertia (kg m^2) (neglected under symmetry assumptions).
$\boldsymbol{I}$	Inertia tensor (kg m^2).
$0_{3\times3}$	3×3 zero matrix.
$\boldsymbol{I}_3$	3×3 identity matrix.
$\boldsymbol{S}(\cdot)$	Skew-symmetric operator.
m_0	Initial glider mass (kg).
$m_b(t)$	Ballast mass at time t (kg).
$m(t)$	Total mass at time t (kg).
$\boldsymbol{r}_g$	Vector from CB to CG in the initial state (m).
$\boldsymbol{r}_b$	Vector from CB to ballast tank CG (m).
$\boldsymbol{I}_0$	Initial inertia tensor (kg m^2).
T_A	Kinetic energy associated with added mass (J).
$\boldsymbol{M}_A$	Added mass matrix.
$\boldsymbol{C}_A$	Added-mass Coriolis/centripetal matrix.
$X_{\dot{u}}, Y_{\dot{v}}, Z_{\dot{w}}, K_{\dot{p}}, M_{\dot{q}}, N_{\dot{r}}$	Added-mass hydrodynamic derivatives (SNAME notation).
$A_{11}, A_{12}, A_{21}, A_{22}$	3×3 block partitions of $\boldsymbol{M}_A$ used in the compact form of $\mathbf{C}_A$.
$\mathrm{d}W_B$	Buoyancy engine work per time step (J).
W_B	Total buoyancy engine work over the mission (J).
$d(t)$	Depth at time t (m).
$\mathrm{d}W_A$	Attitude adjustment work per time step (J).
W_A	Total attitude adjustment work over the mission (J).
$\boldsymbol{x}$	Simulation state vector, includes $\boldsymbol{\eta}$ and $\boldsymbol{\nu}$.
Δt	Numerical integration time step (s).
t_{max}	Maximum simulation time (s).
w_{sp}	Down velocity setpoint (ms^{-1}).
θ_{sp}	Pitch setpoint (rad).
ϕ_{sp}	Roll setpoint (rad).
w_e	Down velocity error (ms^{-1}).
θ_e	Pitch error (rad).
ϕ_e	Roll error (rad).